EPSC2018

MSP2/MD8 abstracts

13 Sep 2018 15:36:45

EPSC Abstracts
Vol. 12, EPSC2018-4, 2018
European Planetary Science Congress 2018

Parametrization of Low Frequency Internal-Gravity Waves in the Shear Flow Driven Ionosphere

Khatuna Chargazia (1,2), Oleg Kharshiladze (2,3), Gaetano Zimbardo (4), Diana Kvatarskhelia (2), Nodar Javakhishvili (2) and Ketevan Gomiashvili (5)
(1) I.Vekua Institute of Applied Mathematics, Iv. Javakhishvili Tbilisi State University, Tbilisi, Georgia (Khatuna.chargazia@gmail.com);
(2) M. Nodia Institute of Geophysics, Iv. Javakhishvili Tbilisi State University, Tbilisi, Georgia;
(3) Physics Department, Iv. Javakhishvili Tbilisi State University, Tbilisi, Georgia;
(4) Department of Astrophysics, University of Calabria, Rende, Italy;
(5) Iv. Javakhishvili Tbilisi State University, Tbilisi, Georgia

Abstract
The linear mechanism of generation, intensification and further nonlinear dynamics of internal gravity waves (IGW) in stably stratified dissipative ionosphere with non-uniform zonal wind (shear flow) is studied. In the ionosphere with the shear flow, a wide range of wave disturbances are produced by the linear effects, when the nonlinear and turbulent ones are absent.

1. Introduction
Internal gravity waves (IGWs) play an important role in the formation of the general circulation, thermal regime, and composition of the middle and upper atmosphere. According to present knowledge, the main portion of IGW energy reaches the middle and upper atmosphere from tropospheric sources. In the middle and upper atmosphere the amplitudes of waves increase, they break and produce substantial amounts of heat and momentum (Holton, 1983).

Several parametrizations have been developed for the turbulent viscosity, mean low drag and heating rates produced by dissipating IGWs (Lindzen, 1981; Matsuno, 1982; Holton, 1983; Gavrilov, 1990; Fritts and Lu, 1992; Medvedev and Klaassen, 1995; Hines, 1997).

One of the important properties of IGW is their significant influence on the distribution of the electromagnetic waves in atmospheric-ionosphere layers. Consequently, ionosphere electric currents and electromagnetic fields may re-influence the wave properties of IGW at ionosphere altitudes.

The results of long-term observations (Kazimirovskii, 1983) also show that at the atmospheric-ionospheric layers the spatially non-uniform zonal winds - the shear flows are permanently present, produced by nonuniform heating of the atmospheric layers by the solar radiation. In this context the problem of the generation and evolution of ordinary and magnetized waves at different layers of the atmosphere during their interaction with non-uniform zonal wind (shear flow) becomes urgent.

In this paper we study the linear evolution of IGW in shear zonal flows (winds) in different regions of the ionosphere. At the initial linear stage in the dynamic equations the perturbed hydrodynamic quantities are given by SFH, which corresponds to non-modal analysis in a moving coordinate system along the background wind. Non-modal mathematical analysis allows replacement of the spatial non-uniform nature of the perturbed quantities, associated with the basic zonal flow, by temporal one in the basic equations and trace the evolution of SFH disturbances according to time.

2. Nonmodal Analysis of IGW
Analysis of the features of magnetized IGW waves at the linear stage in the ionosphere should be conducted in accordance with a non-modal approach. For this purpose, the moving coordinate system $X_1O_1Y_1$ is more convenient with origin $\boldsymbol{O}_1$ and the axis $\boldsymbol{Y}_1$, which coincides with the same characteristics of the equilibrium local system $\boldsymbol{XOY}$, the axis $\boldsymbol{X}_1$ flowing along the unperturbed (background) wind**.** In this reference frame, For each perturbed quantities, we obtain equations for Spatial Fourier Haronics (SFP):

$$\frac{\partial V_x}{\partial \tau} = -SV_z + k_x P - [b_0 + \nu k^2(\tau)]V_x\,, \qquad (1)$$

$$\frac{\partial V_z}{\partial \tau} = k_z(\tau)P - \rho - [b_y + \nu k^2(\tau)]V_z\,, \qquad (2)$$

$$\frac{\partial \rho}{\partial \tau} = V_z \,,\; k_x V_x + k_z(\tau) V_z = 0 \,. \qquad (3)$$

Here, $\mathbf{V} = \mathbf{V}_0(z) + \mathbf{V}(x,z,t)$, $\rho = \rho_0(z) + \rho(x,z,t)$, $P = P_0(z) + P(x,z,t)$, $K^2 = k_x^2 + k_z^2 + 1/(4H^2)$, $K_1^2 = K_2^2 - ik_z / H$, $K_2^2 = k_x^2 + k_z^2 - 1/(4H^2)$, S is a shear parameter - $\mathbf{V}_0(z) = v_0(z)\, \boldsymbol{e}_x = S \cdot z \cdot \boldsymbol{e}_x$.

Normalized energy density of the Fourier harmonics have the following form:

$$\overline{E}(\tau) = \frac{E(\tau)}{E(0)} = \frac{\left(1 + k_0^2\right)^2}{\left[1 + (k_0 - S\tau)^2\right]^{1/2}} \,. \qquad (4)$$

In the initial stage of evolution when $k_0 = k_z(0)/k_x > 0$ (when $k_z(\tau) > 0$) over time τ, $0 < \tau < \tau^* = k_z(0)/(Sk_x)$, in (4) the denominator decreases and, accordingly, the energy density of IGW increases monotonically and reaches its maximum value (exceeding its initial value by an order) at the time $\tau = \tau^*$. Further, at $\tau^* < \tau < \infty$ the energy density begins to decrease (when $k_z(\tau) < 0$), and monotonically returns to its initial approximately constant value. In other words, in the early stages of evolution, temporarily, when $k_z(\tau) > 0$ and IGW perturbations are in the intensification region in wave-number space, the disturbances draw energy from the shear flow and increase own amplitude and energy by an order during the period of time $0 < \tau < \tau^* = k_z(0)/(Sk_x) = 100$. Then (if the nonlinear processes and the self-organization of the wave structures are not turned on), when $k_z(\tau) < 0$, IGW perturbation enters the damping region in wave number space and the perturbation returns energy back to the shear flow over time $\tau^* < \tau < \infty$ and so on. Such transient redistribution of energy in the medium with the shear flow is due to the fact that the wave vector of the perturbation becomes a function of time $k = k(\tau)$, i.e. disturbances' scale splitting takes place. The structures of comparable scales effectively interact and redistribute free energy between them. Taking into account the induction and viscous damping the perturbation's energy reduction in the time interval $\tau^* < \tau < \infty$ is more intensive than that shown on fig. 1, the decay curve in the region $\tau^* < \tau < \infty$ becomes more asymmetric (right-hand side curve becomes steeper), and part of the energy of the shear flow passes to the medium in the form of heat.

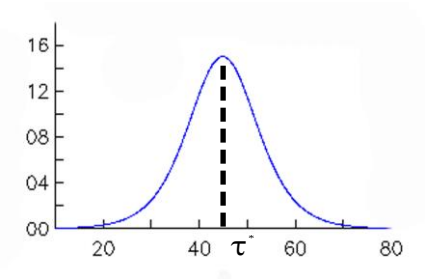

Fig.1

3. Summary and Conclusion

In this article the linear stage of generation and further nonlinear evolution of IGW structures in the dissipative stably stratified ionosphere in the presence of shear flow (non-uniform zonal wind) is studied. A model system of dynamic nonlinear equations describing the interaction of internal gravity structures with viscous ionosphere, non-uniform local zonal wind, and the geomagnetic field is obtained. On the basis of analytical solutions and theoretical analysis of the corresponding system of dynamic equations a new mechanisms of linear transient pumping of shear flow energy into that of the wave perturbation, wave amplification (multiple times) is revealed.

Acknowledgements

Is paper is prepared by the support of the project NFR2017_252 of Shota Rustaveli National Science Foundation.

References

[1] Holton, J:. Journal of Atmospheric Sciences. V 40, P.2497, 1983;
[2] Lindzen, R:. JGR, V. 86, Issue C10, 1981;
[3] Gavrilov N:. J. Atmos. Terr. Phys., V. 52, P. 707, 1990.
[4] Fritts, D. and Luo, Z. J. Atmos. Sci., V. 49, P. 681, 1992.
[5] Medvedev, A. and Klaassen, P. J. Geophys. Res., 100(D12), 25, P. 841, 1995.
[6] Hines, C:. J. Atmos. Solar-Terr. Phys., V. 59, P. 371, 1997.
[7] Kazimirovsky, E:. Nauka Press, Moscow, V. 66, P. 170, 1983.

EPSC Abstracts
Vol. 12, EPSC2018-15, 2018
European Planetary Science Congress 2018

Limit Cycles in a Toy Model of "Earth-like" Magnetotail Dynamics

Robert Burston
University of Bath, Bath, UK, rjb22@bath.ac.uk

Please make sure that your pdf conversion results in a document with a page size of 237 x 180 mm!

Abstract

A toy model of "Earth-like" magnetotail dynamics capable of separately incorporating the Dungey and Vasyliunas Cycles is presented. This makes it applicable to Mercury, Earth, Jupiter and Saturn. The model is also capable of incorporating dynamical noise in the system. No previous model has this level of generality. Evidence is presented of the existence of limit cycles in the dynamics of the model. Limit cycles correspond to periodic behavior but the waveform need not be a simple sinusoid. The presence of limit cycles in the system dynamics implies that under some driving conditions, magnetotail plasmoid formation can be a predictably repeating process.

1. Introduction

The magnetospheres of the planets, Mercury, Earth, Jupiter and Saturn can all be described globally as having a compressed nose on the sunward side, up-stream in the solar wind and a long, stretched magnetotail on the night, down-stream side. When conditions are appropriate all four magnetotails can undergo a cyclical process of plasmoid formation driven either by the solar wind/Dungey Cycle (Mercury, Earth), atmospheric rotation/Vasyliunas Cycle (Jupiter) or both (Saturn) [1]. A toy model describing the dynamics of plasmoid formation, applicable to all of these planets is useful for understanding the variable responses to different driving conditions and how predictable the system is. Such a model is presented here. Although other types of behavior are possible (e.g. stochastic and chaotic modes) the results presented here focus on evidence for the existence of limit cycles (periodic behavior) at certain parameter values. The model is based on the analogy between magnetotail plasmoid formation and the formation of water drops by a leaking tap [2] and is an extension of the Shaw model of a leaky tap [3]. This models the leaky tap as a mass on a spring under gravity, with mass increasing at a constant rate. The analogy between the three systems is close because of the tension force involved; elasticity in the spring, water surface tension in the leaky tap and magnetic tension in the magnetotail.

2. The Model

The model is a form of non-linear relaxation oscillator given by the following equations:

$$F = mg - kx - C_{damp}\frac{dx}{dt} - C_{drag}\left(\frac{dx}{dt}\right)^2 \quad (1)$$

$$\frac{dm}{dt} = C_D \pm w_D + C_V \pm w_V \quad (2)$$

$$\Delta m = C_u \frac{dx}{dt}\Big|_{x=x_c} \quad (3)$$

(1) represents the forces on the spring (from left to right, gravity, the elastic restoring force, damping by heat generation and viscous drag). F is the total force, m is the attached mass (not constant), k is the spring constant, x is the displacement, t is time and C_{damp} and C_{drag} are the damping and drag constants, respectively. (2) describes the continuous rate of change of mass and has four terms. C_D and C_V are the rates of increase of attached mass due to the Dungey and Vasyliunas Cycles, respectively. The time dependence of the values of C_D and C_V may be altered arbitrarily in the model. In this paper, however, each is set to be constant for the whole of any given model run. w_D and w_V are noise terms that modify the values of C_D and C_V. These may be set to zero (purely deterministic case) or to select from any pseudo-random distribution realisable in Matlab at each time step of the model run. These variations represent dynamical noise. (3) represents the instantaneous loss of mass when a plasmoid detaches at the critical

displacement, x_c. Δm is the instantaneous mass lost. C_u is a constant of proportionality that may take any positive finite value but is fixed for any given model run.

3. Results

For some sets of parameter values, the behavior of the model, as viewed in the system phase space, is that of an attracting limit cycle. A limit cycle is a closed loop in phase space. Once on a limit cycle, the system can never escape it. Limit cycles represent periodic behaviour but not necessarily a simple sinusoidal oscillation. An attracting limit cycle is a limit cycle that attracts nearby points in phase space on to it given sufficient time. Figure 1 shows a trajectory in the 3-D phase space of the model presented in section 2, above, that is an example of an attracting limit cycle. As time goes on, points on the trajectory get progressively lighter, as indicated by the colour bar. The trajectory can be seen to settle on a repeating distorted helix at late times. This is the limit cycle. Figure 2 shows the discrete masses lost over time for the same model run as represented in Figure 1. Time is on a log scale to clearly illustrate early behavior. It can be seen that the system rapidly settles into a pattern of releasing identical amounts of mass at constant time intervals. This is analogous to repeatedly forming plasmoids of uniform size at constant time intervals.

Figure 1: This is the example of an included figure.

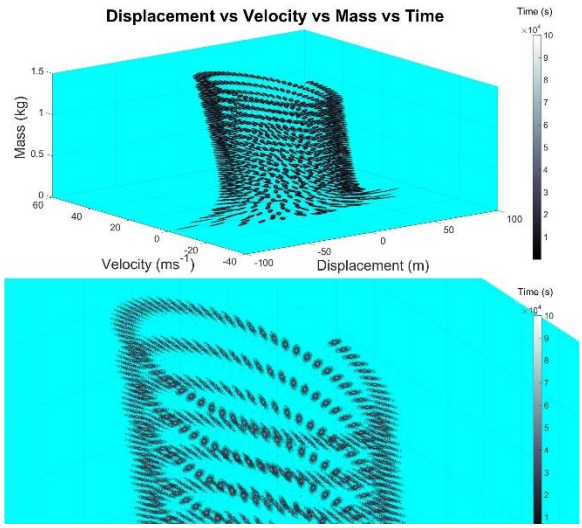

Figure 1: (Above) an attracting limit cycle in the model phase space. (Below) A zoom into the top region of the attracting limit cycle. It can be seen that at late times (lighter points) the trajectory has converged on to the centre of the approximately helical structure. This is the limit cycle.

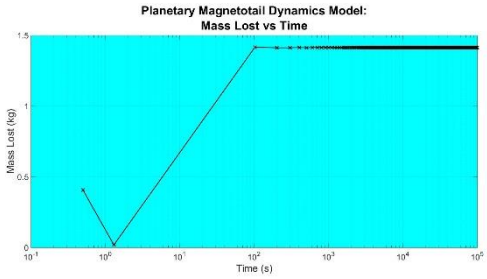

Figure 2: The discrete masses lost as a function of time (log scale). Note the rapid convergence to periodic behavior. The solid black line is an aid to the eye: masses are lost as discrete amounts at times marked by the black X symbol.

4. Conclusions

The model presented has attracting limit cycles in its phase space for some parameter value sets. These correspond to periodic behaviour. When viewed in terms of discrete mass lost, analogous to drops of water in the leaky tap case and plasmoids in the magnetotails case, the behaviour is seen as a brief transient followed by regular release of the same amount of mass at uniform time intervals. This is qualitatively the same as the behaviour of Earth's magnetotail at times of low to moderate substorm activity.

5. Acknowledgements

The author gratefully acknowledges the support of the Science and Technology Facilities Council in supporting this work under grant ST/P004016/1.

References

[1] Keiling, A, Jackman, C and Delamere, P (Eds.): Magnetotails in the Solar System, Wiley/AGU ISBN: 9781118842348, 2015.

[2] Hones, E.: Transient Phenomena in the Magnetotail and their Relation to Substorms, Space Science Reviews, Vol.23, Is. 3, p 393-410, 1979.

[3] Shaw, R.: The Dripping Faucett as a Model Chaotic System, Aerial Press, ISBN: 0942344057, 1984.

EPSC Abstracts
Vol. 12, EPSC2018-100, 2018
European Planetary Science Congress 2018

(A)uroral (K)ilometric (R)adiation as a Self-Organized System

M. Marek, and R. Schreiber
Space Research Centre of the Polish Academy of Sciences, Warsaw, Poland (mmarek@cbk.waw.pl)

Abstract

We present results of the processing of short–time AKR (Auroral Kilometric Radiation) bursts recorded onboard Interball–2 mission (POLRAD experiment). POLRAD was a swept–frequency radio–spectrograph working mostly in the frequency range 4 kHz–1 MHz. Sweep duration with a 4 kHz wide filter was 6 s, but for the single frequency step, data integration time was only 6 ms [1].

Preliminary analysis of the distribution of short AKR bursts number in function of their intensity showed for higher intensities a power–law fall (in a log–log scale) characteristic for the Self–Organized Criticality (SOC) systems [2].

We present here results of analysis for a much larger data sample consisting of 241 data sets (vs. 53 cases in [2]). As in the previous paper, for analysis of the power–law part of the distribution, we applied method proposed by Clauset et al., [3] subsequently discussed for power–law–distributed solar data by D'Huys et al., [4]. We found about 80% of scaling parameters values α within the [2.0-3.0] interval with the dominant value ≈ 2.5. We also compared fits to our data of three different distributions: powerlaw, exponential and lognormal. The powerlaw distribution fits data better than the exponential, but for the powerlaw distribution vs. the lognormal our results are not conclusive.

SOC is a rather general concept, and at first we decided to fit the AKR bursts data to a simple analytical model, the logistic–growth model [5], using AKR waveform data from the French MEMO experiment [6]. Results agree well with the expected growth rates for the AKR cyclotron maser instability.

MEMO data are very scarce, but we can see, that data integrated in a 6 ms time window consist in some cases from more than one AKR burst. Such lack of time resolution can lead to the overestimate of the scaling parameter α [7,8].

Acknowledgements

This research was supported by the Ministry of Science and Higher Education via financing of development of young researchers and doctoral program participants (MM).

References

[1] Hanasz, J. et al., Observation of auroral kilometric radiation on the INTERBALL–2 satellite: the POLRAD experiment, Cosmic Res., 36, 617, 1998.

[2] Marek, M., and R. Schreiber, Is the AKR Cyclotron Maser Instability a self-organized criticality system? in Radio Emissions VIII, edited by G. Fischer, G. Mann, M. Panchenko, and P. Zarka, Austrian Academy of Sciences Press, Vienna, pp. 269-277, 2017.

[3] Clauset, A., C. R. Shalizi, and M. E. J. Newman, Power–law distributions in empirical data. SIAM Rev., 51, pp. 661–703, 2009.

[4] D'Huys, E. et al, The effect of limited sample sizes on the accuracy of the estimated scaling parameter for power–law–distributed solar data, Solar Phys., 291, 1561, 2016.

[5] Aschwanden, M. J., Self–Organized Criticality in Astrophysics, Springer–Verlag, Berlin, Heidelberg, Germany, 2011.

[6] Lefeuvre, F. et al., Preliminary results from the MEMO multicomponent measurements of waves on-board INTERBALL 2, Ann. Geophys. 16, pp. 1117-1136, 1998.

[7] Markus J. Aschwanden et al., 25 Years of Self-Organized Criticality: Solar and Astrophysics, Space Sci. Rev. 198, pp. 47–166, 2016.

[8] Isliker H. and A. O. Benz, On the reliability of peak-flux distributions, with an application to solar flares, Astronomy and Astrophysics, pp. 1040–1048, 2001.

EPSC Abstracts
Vol. 12, EPSC2018-318, 2018
European Planetary Science Congress 2018

Evaluating Single Spacecraft Observations of Planetary Magnetotails with a Simple Monte Carlo Simulation

A. W. Smith (1), C. M. Jackman (1), C. M. Frohmaier (2), J. C. Coxon (1), J. A. Slavin (3) and R. C. Fear (1)
(1) Department of Physics and Astronomy, University of Southampton, Southampton, UK, (2) Institute of Cosmology and Gravitation, University of Portsmouth, Portsmouth, UK, (3) Climate and Space Sciences and Engineering, University of Michigan, Ann Arbor, USA (aw.smith@soton.ac.uk)

Abstract

Surveys are often undertaken of spacecraft magnetometer (and plasma) data to locate various products of reconnection within planetary magnetotails (e.g. flux ropes). These surveys of in-situ data are constrained by both the orbits of the spacecraft and the numerical limits placed upon the required signatures (e.g. field deflections). A simple Monte Carlo model is presented that allows the investigation of the effect of orbital sampling on the inferred distribution of flux ropes. It is found that, for MESSENGER surveys of Mercury's magnetotail, at least 200 orbits are generally required to accurately determine the underlying population. However, this number is a function of both the width of the structures and the precision to which the distribution is required. Fitting Monte Carlo simulations to the results of a recent survey [1] suggests that the center of Mercury's neutral line is offset dawnward of midnight by ~ 0.4 RM. The downtail location of the neutral line is not consistent with previous studies unless dissipation terms are included planetward of the reconnection site. The identification bias caused by various selection criterion are probed by simulating flux ropes using the force-free model. The results are shown with respect to two recent surveys; each can be seen to preferentially select a slightly different subset of the underlying population. Correcting for these effects allows a more complete description of the underlying distribution.

1. References

[1] Smith, A. W., J. A. Slavin, C. M. Jackman, G. K. Poh, and R. C. Fear (2017a), Flux ropes in the Hermean magnetotail: Distribution, properties, and formation, Journal of Geophysical Research: Space Physics, 122(8), 8136–8153, doi:10.1002/2017JA024295.

EPSC Abstracts
Vol. 12, EPSC2018-332, 2018
European Planetary Science Congress 2018

Subsolar magnetopause and cusp positions: comparison of MHD and empirical models

Andrey Samsonov, Graziella Branduardi-Raymont
Mullard Space Science Laboratory, University College London, United Kingdom (a.samsonov@ucl.ac.uk)

Abstract

We simulate temporal variations of the subsolar magnetopause and cusp positions using global magnetohydrodynamic (MHD) models and compare predictions with the corresponding empirical models. In the second part, we calculate X-ray images from the MHD simulations. Results of this work can be used in preparation to the forthcoming SMILE mission.

1. Introduction

Global MHD models have been successfully used in different areas of space and planetary physics, including propagation of transient solar wind structures in the inner heliosphere [1], interaction of the solar wind with the interstellar medium, interaction of the solar wind with the Earth's magnetosphere [2] as well as with other planetary magnetospheres and even moons [3]. The latter paper illustrates that MHD models can be coupled with kinetic models in the regions where kinetic physics is essential for large scale dynamics.

MHD simulations help in studying the magneto-spheric response to solar wind variations. Results of MHD models have been often compared with in-situ measurements [e.g., 4] or alternatively with empirical statistical models [5,6]. In particular, empirical magnetopause models [7,8] based on large databases of magnetopause crossings specify magnetopause shape with analytical functions and deduce relations between solar wind parameters (in [8] also taking into account the dipole tilt) and parameters that characterize the magnetopause shape. In general, global MHD models are in reasonably good agreement with empirical magnetopause models, except that some empirical models predict much stronger variations of magnetopause positions with solar wind parameters and dipole tilt than others [6].

Three stationary solutions were simulated in [6] to compare predictions of the magnetopause positions at subsolar point and in terminator plane. We extend this approach here by simulating an 8-hours solar wind interval on 2 November 2009 and comparing predictions of empirical and MHD models. Moreover, we have studied temporal variations of cusp latitudes in dependence on solar wind conditions.

2. Magnetopause and cusp positions

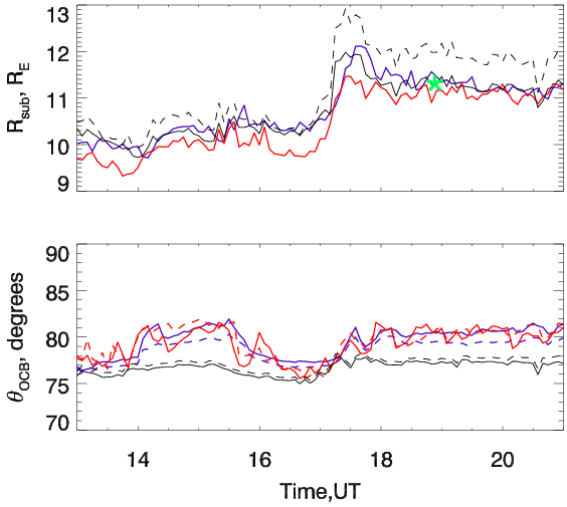

Figure 1: Top: variations of the subsolar magnetopause with time. Blue and red lines correspond to BATSRUS [2] and LFM [9] MHD models respectively, black solid line – Shue et al.'s model [7], black dashed line – Lin et al.'s model [8], green star indicates a THEMIS magnetopause crossing. Bottom: variations of the open-closed boundary (OCB) latitudes with time. Blue and red lines – results of BATSRUS [2] and LFM [9] models, black lines – OCB latitude in empirical models (subsolar point obtained by Shue et al.'s model was traced along field lines by Tsyganenko (T01) magnetospheric model. Solid and dashed lines correspond to the north and south cusps.

Fig. 1 compares the results of MHD simulations with predictions of empirical models. We note a good agreement in predictions of the subsolar magnetopause distance between both MHD models and the empirical Shue et al.'s model, while the Lin et al.'s model predicts a slightly larger magnetopause distance. The predictions of MHD and Shue et al.'s models well agree with the THEMIS magnetopause crossing indicated by the green star. Both MHD models yield quantitatively and qualitatively similar variations in the OCB latitude which corresponds to the south edge of the cusp.

3. X-ray images in MHD simulation

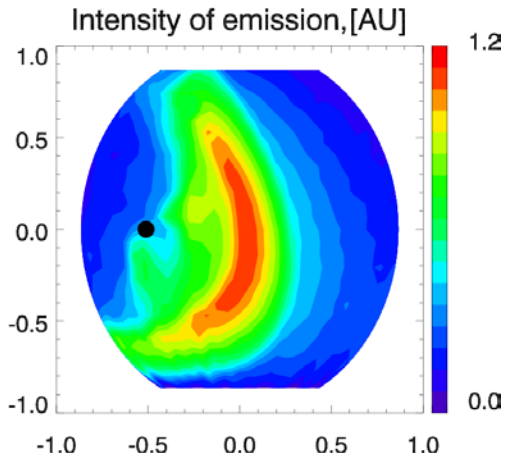

Figure 2. Simulated intensity of X-ray emission at the supposed apogee of SMILE at (6.8, 7.7, 17.1) R_E in GSM coordinates. The center of the image is at the subsolar magnetopause ~10.0 R_E.

Global MHD models predict the spatial distribution of the fluid density and velocity, as well as the position of the magnetopause in any particular time. The intensity of X-ray emission integrated along the line of sight can be calculated as shown below [10]:

$I \approx \int N_{SW} N_H V_{rel} dl$, where N_{SW} – the solar wind ion density, N_H – the exospheric neutral density [11], and V_{rel} – the relative velocity between two species which depends on the solar wind bulk velocity and thermal speed. An example of such calculation is shown in Fig. 2.

References

[1] Odstrcil, D.: Modeling 3-D solar wind structure, Advances in Space Research, Vol. 32, pp. 497-506, 2003.

[2] Tóth, G., et al.: Space Weather Modeling Framework: A new tool for the space science community, Journal of Geophysical Research, Vol. 110, A12226, doi:10.1029/2005JA011126, 2005.

[3] Tóth, G., et al.: Extended magnetohydrodynamics with embedded particle-in-cell simulation of Ganymede's magnetosphere, Journal of Geophysical Research., Vol. 121, pp. 1273–1293, 2016.

[4] Samsonov, A.A., Alexandrova, O., Lacombe, C., Maksimovic, M., and Gary, S. P.: Proton temperature anisotropy in the magnetosheath: comparison of 3-D MHD modelling with Cluster data, Annales Geophysicae, Vol. 25, pp. 1157-1173, 2007.

[5] Gordeev, E., et al.: Assessing the performance of community-available global MHD models using key system parameters and empirical relationships, Space Weather, Vol.13, pp. 868-884, 2015.

[6] Samsonov, A.A., et al.: Do we know the actual magnetopause position for typical solar wind conditions? Journal of Geophysical Research, Vol.121, pp. 6493–6508, 2016.

[7] Shue, J.-H. et al.: Magnetopause location under extreme solar wind conditions, Journal of Geophysical Research, Vol. 103, pp. 17691–17700, 1998.

[8] Lin, R.L., Zhang, X.X., Liu, S.Q., Wang, Y. L., and Gong, J.C.: A three-dimensional asymmetric magneto-pause model, Journal of Geophysical Research, Vol. 115, A04207, doi:10.1029/2009JA014235, 2010.

[9] Lyon, J.G., Fedder, J.A., and Mobarry, C.M.: The Lyon-Fedder-Mobarry (LFM) global MHD magneto-spheric simulation code, Journal of Atmospheric and Solar-Terrestrial Physics, Vol. 66, pp. 1333-1350, 2004.

[10] Sibeck, D.G. et al.: Imaging Solar Wind Interactions in Soft X-rays, Space Science Reviewers (in press).

[11] Østgaard, N.; Mende, S. B.; Frey, H. U.; Gladstone, G. R.; Lauche, H.: Neutral hydrogen density profiles derived from geocoronal imaging, Journal of Geophysical Research, Vol. 108, doi: 10.1029/2002JA009749, 2003.

EPSC Abstracts
Vol. 12, EPSC2018-350, 2018
European Planetary Science Congress 2018

Constraining Ganymede's exosphere through numerical simulations of its ionosphere and Galileo observations

Gianluca Carnielli (1), Marina Galand (1), Ronan Modolo (2), François Leblanc (3), Arnaud Beth (1), Hans L. F. Huybrighs (4,5,6), Xianzhe Jia (7)
(1) Department of Physics, Prince Consort Road, Imperial College London, London SW7 2AZ, UK (gianluca.carnielli10@imperial.ac.uk), (2) LATMOS/IPSL, UVSQ Université Paris-Saclay, UPMC Univ. Paris 06, Guyancourt, France, (3) LATMOS/IPSL, CNRS, Sorbonne Université, UVSQ, Paris, France (4) Max-Planck-Institut für Sonnensystemforschung, Göttingen, Germany, (5) Swedish Institute of Space Physics, Post Office Box 812, Kiruna, Sweden, (6) Institut für Geophysik und extraterrestrische Physik, Technische Universität, Germany, (7) Department of Climate and Space Sciences and Engineering, University of Michigan, Ann Arbor, MI 48109-2143, USA

Abstract

Our current understanding of Ganymede's neutral environment derives from models which are driven by a limited set of observations. These include remote sensing UV measurements from close flybys by the Galileo and Voyager spacecraft and from Earth by the Hubble Space Telescope (HST).

Estimated parameters from observations include the column density of H [1,2] and O_2 [2,3]. For O_2, we argue that the derivation of the column density was based on strong assumptions on the plasma environment, which is poorly characterized. These estimates have been used as reference values in exospheric models (e.g. [4,5,6]), but cannot be confirmed without additional in situ measurements, which will be made by the JUICE spacecraft during the late phase of the mission.

One way to check the consistency between the estimated column density of the neutral species and Galileo observations, is to develop a model of Ganymede's ionosphere, starting from an exosphere which reproduces the estimated column densities, and check that the plasma properties derived by the model along the flyby trajectories correspond to those measured by Galileo.

We have developed such a model for Ganymede [7] using the exospheric configuration from Leblanc et al. (2018) [4], which reproduces the O_2 column density estimated by Hall et al. (1998) [3]. For the plasma number density along the Galileo flyby trajectories, the model underestimates by more than one order of magnitude the observations. We attribute the cause of this discrepancy to the assumed configuration of the neutral exosphere, which we argue to be underestimated.

Here, we present a new possible configuration of the O_2 exosphere which leads to a plasma density in the ionospheric model that is consistent with that measured by Galileo along the close flyby trajectories. To reach agreement, we had to increase the column density of O_2 from the original estimate of Hall et al. (1998) [3].

We conclude that overall Ganymede's O_2 exosphere should be denser than what has been assumed so far.

Acknowledgements

We warmly acknowledge the support of the IPSL data centre CICLAD for providing access to their computing resources. Work at Imperial College London was supported by STFC of UK through a postgraduate studentship and under grants ST/K001051/1 and ST/N000692/1.

References

[1] Barth, C.A., Hord, C.W., Stewart, A.I.F., Pryor, W.R., Simmons K.E., McClintock, W.E., Ajello, J.M., Naviaux, K.L. and Aiello, J.J.: Galileo ultraviolet spectrometer observations of atomic hydrogen in the atmosphere at Ganymede, Geophysical Research Letters, Vol. 24, p. 2147, 1997.

[2] Feldman, P.D., McGrath, M.A., Strobel, D.F., Moos, H.W., Retherford, K.D. and Wolven, B.C.: HST/STIS Ultraviolet Imaging of Polar Aurora on Ganymede, The Astrophysical Journal, Vol. 535, pp. 1085-1090, 2000

[3] Hall, D.T., Feldman, P.D., McGrath, M.A. and Strobel, D.F.: The Far-Ultraviolet Oxygen Airglow of Europa and

Ganymede, The Astrophysical Journal, Vol. 499, pp. 475-481, 1998

[4] Leblanc, F., Oza, A.V., Leclercq, L., Schmidt, C., Cassidy, T., Modolo, R., Chaufray, J.Y. and Johnson, R.E.: On the orbital variability of Ganymede's atmosphere, Icarus, Vol. 293, pp. 185-198, 2018

[5] Marconi, M.L.: A kinetic model of Ganymede's atmosphere, Icarus, Vol. 190, pp. 155-174, 2007

[6] Turc, L., Leclercq, L., Leblanc, F., Modolo, R. and Chaufray, J.Y.: Modelling Ganymede's neutral environment: A 3D test-particle simulation, Icarus, Vol. 229, pp. 157-169, 2014

[7] Carnielli, G., Galand, M., Leblanc, F., Leclercq, L., Modolo, R., Beth, A., Huybrighs, H.L.F., Jia, X.: First 3D test particle model of Ganymede's ionosphere, Icarus, under review

EPSC Abstracts
Vol. 12, EPSC2018-513, 2018
European Planetary Science Congress 2018

Modeling of kinetic wave modes for various magnetospheric conditions at Jupiter

Sascha Janser (1) and Joachim Saur (1)
(1) Institute for Geophysics and Meteorology, Cologne, Germany (sjanser@smail.uni-koeln.de)

Abstract

Jupiter's aurora has been subject of scientific interest for decades. The current JUNO mission investigates the magnetospheric environment of Jupiter and in particular its polar region, which has not been probed by previous spacecrafts. First observations have now revealed that the electron energization processes in the acceleration region of the main aurora are more complex than expected. Therefore we investigate wave-particle interactions by different dissipative and dispersive wave modes in the kinetic regime. These are thought to be an energization mechanism to power auroral electrons. We model the propagation properties of different wave modes by solving the hot plasma dispersion relation for various magnetospheric conditions at Jupiter and aim to find a suitable wave candidate for further investigation of stochastic acceleration processes.

EPSC Abstracts
Vol. 12, EPSC2018-619, 2018
European Planetary Science Congress 2018

Imaging of energetic neutral atoms with the Jovian Neutral Atoms Analyser onboard JUICE: Charge exchange ENAs near Ganymede

M.B. Neuland (1), Y. Futaana (1), S. Fatemi (1), M. Shimoyama (1), A. Vorburger (2), P. Wurz (2), M. Wieser (1) and S. Barabash (1)

(1) Institutet för rymdfysik, IRF, Rymdcampus 1, SE - 98128 Kiruna, Sweden
(2) University of Bern, Physics Institute, Space Research and Planetary Sciences, Sidlerstrasse 5, CH – 3012 Bern, Switzerland

Abstract

The Jovian Neutral Atoms Analyser (JNA) is one of the sensors of the Particle Environment Package (PEP) for the JUICE mission. Mapping of the energetic neutral atoms (ENAs) in the Ganymede magnetosphere, will offer valuable clues about the interaction of the Jovian plasma with the icy moon's surface and the magnetospheric plasma processes. We will present expectations of neutral fluxes, particularly neutrals produced via charge exchange, in the vicinity of Ganymede. From these expectations from our model we infer the expectations for JNA measurements.

1. Introduction

The Jovian system is subject to complex plasma physics processes and can therefore be considered as a giant particle accelerator. Due to the plasma interactions, the Jovian moons are affected by diverse processes that lead to a vast range of space weathering effects and to a constant mass input to the environment of the moons.
Ganymede possesses a strong intrinsic magnetic field that imposes restrictions on the possible trajectories of plasma ions in the Ganymede magnetosphere [1]. As a result, certain terrains on the surface of the Jovian moon are protected against space weathering processes while others are not.

The JNA onboard the JUICE spacecraft will measure energetic neutral light and heavy atoms in an energy range from 10eV to 3keV [2], which covers the energy range of ENAs emanating from various different ENA production mechanisms. Low energy ENAs produced via sputtering and backscattering will be used to image the precipitation regions and, in particular, the boundary of open and closed field lines. In addition, ENAs are expected to be produced by the charge – exchange mechanism in the vicinity of Ganymede due to the presence of the moon's exosphere. From the measurement of these ENAs, we can infer the global plasma distribution in the Ganymede magnetosphere.
In this study we investigate the interaction between the Jovian plasma and the Ganymede magnetosphere and exosphere. In the Jovian system these interactions of the co-rotating magnetospheric plasma with the icy moons give rise to several observative effects, like for example the UV-aurorae observed on Ganymede [6].
The energy balance in terms of mass and radiation balance is one key scientific question of the mission as well as the surface and exosphere composition of the Jovian moons [4]. The direct measurements of mass flux by the JNA will undoubtedly contribute to answer these questions.

2. Model

To calculate the expected fluxes of ENAs, and particularly those resulting from the charge exchange processes, we combined the plasma spatial and velocity distribution modelled by hybrid simulation [5], the exospheric density model for Ganymede [8], and the charge exchange cross sections [7].

The simulations were run for hydrogen and oxygen, since these are the prominent species, particularly in the energy range covered by the JNA measurements. Fig. 1 shows the locations of hydrogen plasma particles from [5] in the GPhiO system as a snapshot in time. The co-rotating Jovian plasma precipitates on the Ganymede magnetosphere from the rear (from $-x$ direction), causing a void in front of the moon, seen in direction of its trajectory along the orbit.

Placing a virtual JNA instrument in the simulation, we can, under consideration of the JNA performance, derive a prediction of the expected neutral fluxes in the instrument. Our studies are a crucial contribution to the planning of the JNA mission operation and to the preparation of the PEP instruments for Ganymede science.

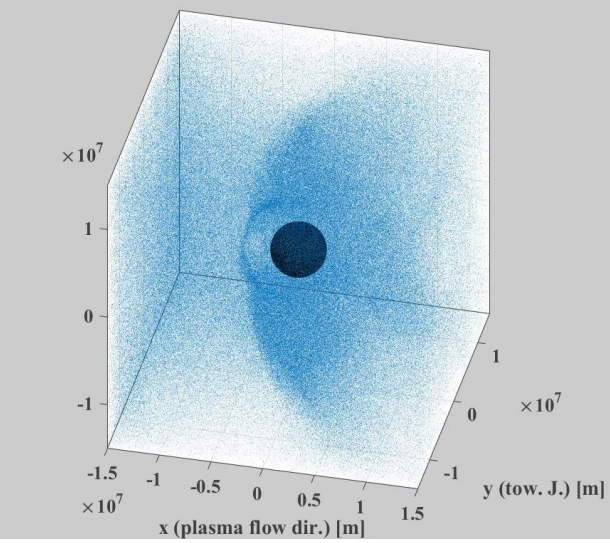

Figure 1 *Spatial distribution of H^+ in the vicinity of Ganymede, reproduced from [5]. Shown in the GPhiO system, the Jovian plasma flow is in +x direction and Jupiter is located towards + y.*

3. Summary

The JNA instrument, one of the sensors of the PEP scientific payload on the JUICE mission, will measure ENAs in the Ganymede magnetosphere and exosphere. These measurements will greatly contribute to our understanding of the interaction of the Jovian plasma with Ganymede, its icy surface and its intrinsic magnetic field. Based on a hybrid model we derived the neutral fluxes produced by charge exchange processes of high energetic plasma particles and neutral atoms in the Ganymede exosphere and the resulting fluxes expected to be measured by the JNA. We present our model, the resulting observations and the ENA fluxes along the JUICE Ganymede orbit expected to be measured by the JNA instrument.

Acknowledgements

This work is supported by the Swiss National Science Foundation (SNF) Early PostDoc Mobility Grant No.168708 and Rymdstyrelsen, the Swedish National Space Board (SNSB).

References

[1] **M.G. Kivelson, K.K. Khurana and M. Volwerk**, The Permanent and Inductive Magnetic Moments of Ganymede, Icarus 157, 2002.

[2] **O. Grasset et al.**, Jupiter Icy moons Explorer (JUICE): An ESA mission to orbit Ganymede and to characterise the Jupiter system, Planet. Space Sci.78, 2013.

[3] **M. Wieser et al.**, Emission of energetic neutral atoms from water ice under Ganymede surface-like conditions, Icarus 269, 2016.

[4] **J.J. Plaut et al.**, Jupiter Icy moons Explorer (JUICE): Science objectives, mission and instruments, 45th Lunar and Planetary Science Conference 2717, 2014.

[5] **Fatemi et al.**, On the formation of Ganymede`s surface brightness asymmetries: Kinetic simulations of Ganymede`s magnetosphere, Geophys. Res. Lett. 43(10), 2016.

[6] **P.D. Feldman et al**., HST/STIS Ultraviolet Imaging of Polar Aurora on Ganymede, Astrophy. J. 535 (2), 2000.

[7] **Scherer et al.**, Ionization rates in the heliosheath and in astrosheaths - Spatial dependence and dynamical relevance, Astronomy & Astrophysics 563, 2014.

[8] **P. Wurz et al.**, The Exospheres of Europa, Ganymede and Callisto, Conference paper, Exo - Climes III, Bern/Switzerland, March 2014

EPSC Abstracts
Vol. 12, EPSC2018-1257, 2018
European Planetary Science Congress 2018

Magneto-convection scaling in the Terrestrial planets

Sergey Starchenko
IZMIRAN, Russia (sstarchenko@mail.ru)

Abstract

Previously two-decade promising numerical planetary MHD dynamo-like first principal modeling has troubles nowadays in its' parameter space. It is been very far from realistic also gives doubtful access to the true physical scales and values via the known scaling laws. Here I have analytically reintroduced/supplemented those laws and suggested hopefully correct and new ones. Under viscosity ν control, I outline suitable parameter space and supplement simple magnetic laws with magnetic energy ρb^2 exiting kinetic ρu^2 one. In the opposite – inviscid limit I have comparable energies in the frame of such one-scale balances. The one-scale viscous and my two-scale balances are compatible with the Christensen-Aubert magnetic law [1] up to moderate magnetic domination. Further, on the way to the powerful fast rotating and diffusion-free planetary-type dynamos, I've got scaling laws with strong magnetic dominations those should as well obey to the known after Rhines [2] pure hydrodynamic scaling. Thus, contrasting to the mainstream I advocate sufficient influence of the inertia and isolate it integrating the radial component of the curl of the momentum equation. In inviscid limit this 2D integral-condition gives balance between magnetic and inertia terms in contrast to the zeroing 1D Taylor condition [3]. Similarly, I manipulated with 0-1-2-3D two-three term balances in the dynamo-equations for correct analytical scaling. On this way, I introduced a variety of typical values those have clear physical and prognostic meaning matching well to the previously observed/estimated magnetic and hydrodynamic values inside the Earth, planets and moons of the Terrestrial type.

Order of magnitude estimations

Convective power F via density anomaly c:

$$F=cug. \qquad (-1)$$

ONE-SCALE SCALINGS

Viscous and magnetically dominated scaling

$$b^2/h^2 = \nu u/h^3 > u^2/h^2. \qquad (0a,b)$$

$$cg/h = \nu u/h^3 = \Omega u/H. \qquad (1a,b,c)$$

The above gives us scaling laws for the small scale h, velocity u and scaled as velocity magnetic field b:

$$h = HE^{1/3},\ u = (F/\Omega)^{1/2}/E^{1/6},\ b = (F\nu)^{1/4}. \qquad (2a,b,c)$$

Large 'viscous' magnetic/kinetic energy ratio:

$$(b/u)^2 = E^{5/6}/S^{1/2} > 1,\ \ S \equiv F/\Omega^3 H^2. \qquad (3a,b,c)$$

Inviscid scaling with magnetic ~ kinetic energy

$$b^2/h^2 = \nu u/h^3 > u^2/h^2. \qquad (4a,b,c)$$

$$cg/h = u^2/h^2 = \Omega u/H. \qquad (5a,b,c)$$

$$h = S^{1/5}H,\ u = S^{2/5}H\Omega = b. \qquad (6a,b,c)$$

Inviscid condition via Rayleigh and Ekman numbers:

$$S > E^{5/3}. \qquad (7)$$

TWO-SCALE INVISCID SCALINGS

Additional Lorentz force scale $l > h$ gives us

$$b^2/l^2 = u^2/h^2 > \nu u/h^3. \qquad (8a,b,c)$$

Energy eqs & sinus s of angle between **U** and **B** give

$$F = sub^2/l. \qquad (9)$$

Moderate magnetic domination scaling

Christensen-Aubert (2006) law [1] works here only if

$$s = l^2/Hh. \quad (10)$$

Additional to (6-7) scaling laws for typical values:

$$b = S^{1/3}H\Omega,\ l = S^{2/15}H,\ s = S^{1/15}. \quad (11a,b,c)$$

Moderate (~10 for the Earth) magnetic domination:

$$(b/u)^2 = 1/S^{2/15}. \quad (12)$$

Strong magnetic domination scaling

Scaling out **B** and rewriting (5) I have *s*-estimation:

$$cg = \Omega us,\ cg/h = \Omega u/H,\ s = h/H. \quad (13a,b,c)$$

Additional to (6-7) scaling laws for typical values:

$$b = S^{1/5}H\Omega,\ l = H,\ s = S^{1/5}. \quad (14a,b,c)$$

Thus, the Lorentz force has the largest scale H and ratio of magnetic to kinetic energy is very large

$$(b/u)^2 = 1/S^{2/5}. \quad (15)$$

Summary and Conclusions

The major result of this paper is inequality (7) that provides us with the guide through various scaling laws to the truly inviscid and diffusion-free MHD dynamos in the Terrestrial planets. Brief outlook on the available simple and advanced numerical geodynamo-like models places them just partly in favor to (7). Thus, the remaining majority is viscosity and diffusivity controlled as [4-5] showed it for simple-type models. Even the domination of magnetic energy over the kinetic one will not guaranty approaching to the inviscid limit because this is a natural feature of the viscous control under the fast rotation due to (13b). That is opposite to (7). Moreover, it is easy to show that the viscosity from the standard mixing-length theory [6] putted into my new pure viscous magnetic law (2c) give us "inviscid" Christensen and Aubert law [1].

The next important result is obtaining of new one-scale and two-scale sets of scaling laws. Those sets of laws are all sufficiently dependant on the inertia in contrast to the mainstream that is under the flag of the Taylor (1963) condition [3]. Using the considered laws of me one could easy to see that even the detailed here Taylor 1D condition could hardly satisfy to the classical $T \approx 0$ at some rather realistic geodynamo parameters. On top of that, my 2D vector condition (7) directly requires involving inertia into the force balance and there is only one alternative to this – viscous control.

The last but not least important result is that various laws obtained here could serve for different Terrestrial planets, (after some correspondent update) Giant planets and fast rotating stars. One-scale inviscid laws could be used for Mercury and Ganymede where magnetic field value is relatively small. Two-scale laws could be suitable for the geodynamo-like systems, Gas Giants (Jupiter, Saturn and correspondent exoplanets) and the stars. Finally viscous control dynamo laws could be suitable for the Icy Giants.

Acknowledgements

This work was basically supported by IZMIRAN budget. Partial supports were by the Russian Foundation for Basic Research with project No 16-05-00507a (geodynamo magnetism) and by 28th program of the Presidium of Russian Academy of Sciences (planetary magnetism).

References

[1] Christensen, U.R., Aubert, J., 2006. Scaling properties of convection-driven dynamos in rotating spherical shells and application to planetary magnetic fields. *Geophys. J. Int.*, 166, 97–114.

[2] Rhines, P.B., 1975. Waves and turbulence on a beta plane. *J. Fluid Mech*., 69, 417–433.

[3] Taylor, J.B., 1963. Magneto-hydrodynamics of a rotating fluid and Earths dynamo problem. *Proc. Roy. Soc.*, A9, 274–283.

[4] King, E.M., Buffett, B.A., 2013. Flow speeds and length scales in geodynamo models: The role of viscosity. *Earth Planet. Sci. Lett.,* 371, 156–162.

[5] Cheng, J.S., Aurnou, J.M., 2016. Tests of diffusion-free scaling behaviors in numerical dynamo datasets. *Earth and Planetary Science Letters*, 436, 121–129.

[6] Starchenko, S.V., Jones, C.A., 2002. Typical velocities and magnetic field strengths in planetary interiors. *Icarus*, 157, 426–435.